

Article

Comparative Study of the Thermal and Hydraulic Performance of Supercritical CO₂ and Water in Microchannels Based on Entropy Generation

Yi Tu ¹  and Yu Zeng ^{2,*} 

¹ Hunan Key Laboratory of Distributed Electric Propulsion Vehicle Control Technology, Hunan University of Arts and Sciences, Changde 415000, China

² School of Aeronautic Science and Engineering, Beihang University, Beijing 100191, China

* Correspondence: zengyu@buaa.edu.cn; Tel.: +86-186-1840-5545

Abstract: The excellent thermophysical properties of supercritical CO₂ (sCO₂) close to the pseudocritical point make it possible to replace water as the coolant of microchannels in application of a high heat flux radiator. The computational fluid dynamics (CFD) method verified by experimental data is used to make a comparison of the thermal hydraulic behavior in CO₂-cooled and of water-cooled microchannels. The operation conditions of the CO₂-based cooling cases cover the pseudocritical point (with the inlet temperature range of 306~320 K and the working pressure of 8 MPa), and the water-based cooling case has an inlet temperature of 308 K at the working pressure of 0.1 MPa. The channel types include the straight and zigzag microchannels with 90°, 120°, and 150° bending angles, respectively. The analysis result shows that, only when the state of CO₂ is close to the pseudocritical point, the sCO₂-cooled microchannel is of a higher average heat convection coefficient and a lower average temperature of the heated surface compared to the water-cooled microchannel. The entropy generation rate of the sCO₂-cooled microchannel can reach 0.58~0.69 times that of the entropy generation rate for the water-cooled microchannel. Adopting the zigzag structure can enhance the heat transfer, but it does not improve the comprehensive performance represented by the entropy generation rate in the sCO₂-cooled microchannel.

Keywords: heat transfer; entropy generation rate; supercritical CO₂; computational fluid dynamics; microchannel



Citation: Tu, Y.; Zeng, Y.

Comparative Study of the Thermal and Hydraulic Performance of Supercritical CO₂ and Water in Microchannels Based on Entropy Generation. *Entropy* **2022**, *24*, 1312. <https://doi.org/10.3390/e24091312>

Academic Editors: Fabio Polonara, Sandro Nizetic, Vítor António Ferreira da Costa and Alice Mugnini

Received: 18 August 2022

Accepted: 15 September 2022

Published: 16 September 2022

Publisher's Note: MDPI stays neutral with regard to jurisdictional claims in published maps and institutional affiliations.



Copyright: © 2022 by the authors. Licensee MDPI, Basel, Switzerland. This article is an open access article distributed under the terms and conditions of the Creative Commons Attribution (CC BY) license (<https://creativecommons.org/licenses/by/4.0/>).

1. Introduction

With the development of electronic equipment in miniaturization and high integration, high heat flux generation poses a greater challenge to the heat dissipation of equipment. There are various potential solutions that have been proposed as potential candidates for electronic cooling, such as impinging jet cooling technology [1,2], heat pipes [3,4], the application of porous materials which can provide a high heat exchange area to volume ratio [5–7], as well as microchannel heat exchangers. The use of microchannels is one of the most important solutions for the design of compact heat sinks for high heat flux removal. Tuckerman and Pease [8] first proposed and tested microchannel heat exchangers and realized heat dissipation with 790 W/cm² for a silicon integrated circuit using water as a coolant. Although microchannel heat exchangers have a surprising heat dissipation capacity, they also have high pumping power requirements due to the high flow resistance of the microchannels [9].

Investigations have been conducted to improve the thermo-hydraulic performance of microchannel heat exchangers, focusing mainly on two directions: one to improve the geometric structure of the microchannel, and the other to find high-performance coolants. Mohammed Adham [10] and Khoshvaght-Aliabadi [11] have investigated the effect of the geometry of the microchannel heat exchanger on its hydraulic and heat

dissipation performance using water as coolant. In their research, the types of triangular, trapezoidal, and sinusoidal channels are compared, and the results indicated that the sinusoidal channel is of the top value of the ratio of average heat convection coefficient to power of pump. Xu et al. [12] suggested a kind of multilayer fractal silicon-based microchannel to optimize the overall pressure drop of the microchannel through step-by-step bifurcation and stratification. Wang et al. [13] studied the effect of geometry parameters on the thermo-hydraulic performance of rectangular microchannels, such as aspect ratio, and found that microchannels show optimum effects with an aspect ratio between 8.904 and 11.442. Song et al. [14] also conducted similar research on trapezoidal microchannels. Kim [15] investigated the validity of the Nu correlation based on the normal channel size to analyze the thermo-hydraulic performance of the microchannel using water as a coolant. The research result showed that the predicted value of Nu by the traditional theoretical correlation model is only reasonable if $Re > 180$ and the aspect ratio > 1 . Peng et al. [16] examined the thermal and hydraulic performance of the zigzag experiment microchannels at four different angles (30° , 45° , 60° , 90°) using deionized water as the working fluid. Numerical analysis with experimental verification is also an important and efficient research method. B. Xu et al. [17] tested the flow characteristics in microchannels with hydraulic diameters ranging from $30\ \mu\text{m}$ to $344\ \mu\text{m}$, and the analysis results showed that the Navier–Stokes formula is able to precisely predict the flow characteristics in the microchannel. Ramos-Alvarado et al. [18] deeply analyzed the impact of channel configurations on the pressure loss as well as the uniformity of the microchannel heat exchanger temperature based on the CFD method. Sohankar et al. [19] investigated how the aspect ratio of the cross section numerically affects the thermal hydraulic characteristics of the rotating rectangular U-shaped microchannel.

To improve the thermo-hydraulic performance of microchannel radiators, the use of better performance coolants is also one of the key research directions. The application of nanofluid as a cooling medium is one of the major branches of research. In this line of study, the heat transfer characteristics of various nanofluids in microchannels have been studied, including Al_2O_3 [20], CuO [21], TiO_2 [22], $\text{Cu-Al}_2\text{O}_3$ [23], and ZnO nanofluid [24]. Chein and Chuang [25] studied the performance of a microchannel radiator with a $\text{CuO-H}_2\text{O}$ mixed coolant. Their research indicates that nanofluids can absorb more heat than water cooling when both are at low flow rates, while in the case of high flow, the thermal performance is mainly determined by the volumetric flow rate, in addition to that the nanoparticles have little effect in this process. Jung and Park [26] conducted an experimental comparative investigation on the thermo-hydraulic performance of Al_2O_3 -water nanofluid in microchannels. Their results indicated that the entropy generation rate of nanofluid is 6.3% lower than that of water, while water has a lower flow resistance. The result also indicated that nanofluids present preferable heat transfer characteristics to water, but their channel pressure loss is not dominant compared to that of water.

CO_2 is a coolant with excellent potential for application in high heat flux dissipation. As a coolant, CO_2 possesses high thermal conductivity and specific thermal conductivity near the pseudocritical point, which is conducive for improving the heat transfer performance [27,28]. Furthermore, as shown in Figure 1, where the data are derived from the RERPROP V9.1 database, the density of CO_2 near the pseudocritical point stays close to that of water, but its dynamic viscosity is significantly lower. These thermophysical characteristics of CO_2 show the potential to improve flow resistance characteristics while maintaining a heat transfer performance close to that of water. Research in [29,30] both showed that supercritical CO_2 (sCO_2) can provide a higher cooling performance with lower channel pressure loss than liquid cooling. Khalesi and Sarunac [31] conducted a good deal of analyses on the development process and conjugated heat transfer in microchannels using supercritical CO_2 and liquid sodium as coolants. Their results showed that the sharp change in the thermophysical property of sCO_2 near the pseudocritical point will impact the flow and thermo-hydraulic performance in the microchannels, and this effect will be weakened with the operational conditions being further away from the critical point.

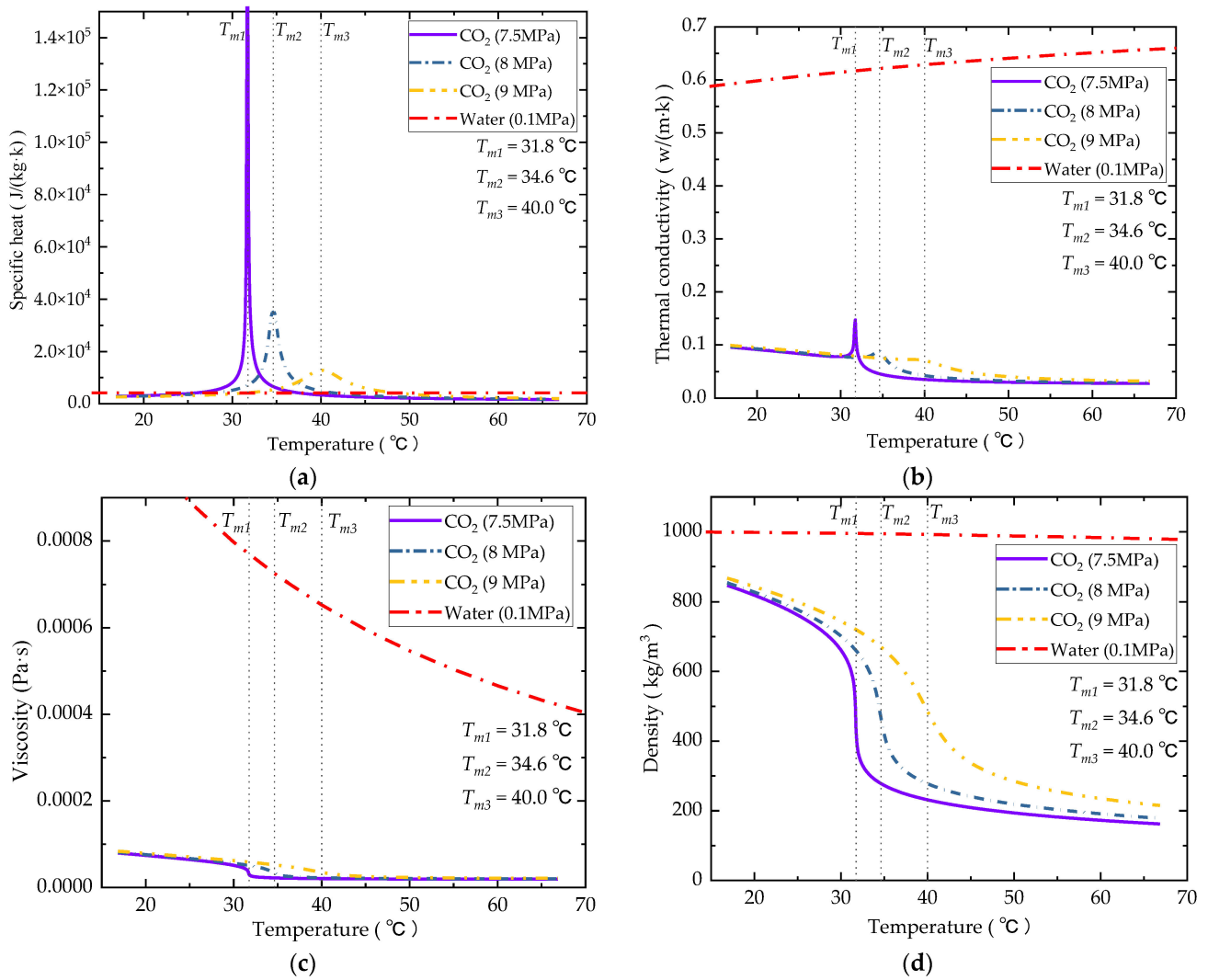


Figure 1. Thermophysical properties of CO₂ at different working pressure (7.5, 8.0, and 9 MPa). (a) Specific heat; (b) thermal conductivity; (c) dynamic viscosity; (d) density.

The results of existing research show that the sCO₂ coolant can provide a higher cooling performance with a lower channel pressure loss compared to the liquid coolant. However, since the thermophysical properties of CO₂ vary sharply near the pseudocritical point, the impact of fluid temperature and pressure change in the microchannel on its thermo-hydraulic performance has not been clearly clarified in existing research. The density of sCO₂ is lower than water, and the pump power consumption of the microchannel heat exchanger is also affected by the density of the fluid, which is one of the parameters that affects the comprehensive performance of the microchannel heat exchanger. In high heat flux heat dissipation applications, it is often desirable to achieve better heat transfer performance with smaller package volume and lower flow resistance (pump power consumption). In this paper, the flow and heat transfer performance of water and CO₂ coolants in microchannels are comprehensively compared based on the entropy generation rate. Special channels such as zigzag [32], curve [33], and trapezoid [34] are important ways to improve thermal performance in the microchannel. A comparison analysis of the effect of the bend angle on the thermal hydraulic performance is also conducted in this study for water and sCO₂-cooled channels.

2. Numerical Method

In this study, water and sCO₂ are used as coolants to study their thermo-hydraulic performance in microchannels. The numerical simulation employs the software ANSYS fluent V19.0 to solve the conjugate heat transfer problem and the Navier–Stokes equations for the computational domains. The SST- $k\omega$ model was used to model turbulence. The pressure-based solver with pressure–velocity coupling was used to solve the flow problem through the ANSYS FLUENT package. The thermophysical characteristics of CO₂ are based on the NIST real gas model with the REFPROP V9.1 database.

2.1. Physical Model and Boundary Conditions

The geometrical model of the microchannel radiator in this analysis is illustrated in Figure 2. The material of this radiator is copper and there are 10 microchannels in total. The width, height, and depth of the radiator is 15 mm × 10 mm × 40 mm. The width and height of the fluid domain is 0.5 mm × 5 mm. In this study, it is assumed that the design of the heat sink header can ensure sufficient uniformity of the fluid in each channel.

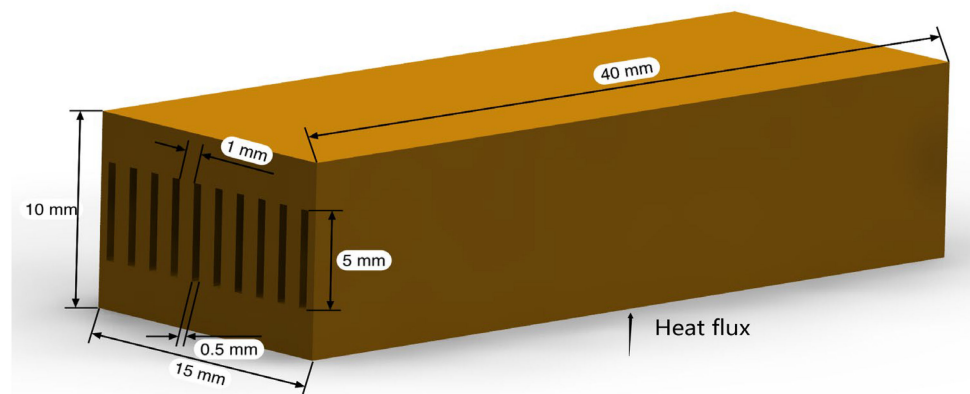


Figure 2. Physical model.

The working boundary conditions for the two fluids are given in Table 1. To make CO₂ work near the pseudocritical point, the outlet pressure of the channels is set at 8 MPa. In this study, a variety of input temperatures (306 K to 320 K) are used to understand the impact of deviation from the pseudocritical point on its thermo-hydraulic performance. Since the temperature and pressure of liquid water have a minor effect on its thermophysical properties, a single inlet temperature (308 K) and a single outlet pressure (0.1 MPa) are adopted. The uniform flow inlet boundary with variation range of mass flux 50~1000 kg/(m²·s) are adopted for both fluid-type conditions. The heat flux ranges from 40,000 to 120,000 W/m² for the heated surface on the bottom side of the solid domain, the coupled heat transfer boundary is adopted at the interface between the fluid and solid regions, and the adiabatic boundary is used for the rest surfaces of the solid domain.

Table 1. Boundary conditions for both coolants.

Coolants	G (kg/(m ² ·s))	P_{out} (MPa)	Q_w (W/m ²)	T_{in} (K)
sCO ₂	50~1000	8	40,000~120,000	306, 307, 308, 310, 315, 320
water	50~1000	0.1	40,000~120,000	308

2.2. Governing Equations and Data Reduction

The continuity, momentum, and energy equations for steady-state flow of the computation fluid domain are expressed as Equations (1)–(3) [35], which are solved by the commercial code ANSYS Fluent. Radiation is not considered in the energy solution. The

buoyancy effect is ignored in this analysis of internal forced convection, as the Richardson number is far less than 0.1 even under the condition of minimum mass flux.

$$\frac{\partial}{\partial x_i} \rho u_i = 0 \quad (1)$$

$$\frac{\partial}{\partial x_j} \rho u_i u_j = -\frac{\partial p}{\partial x_i} + \frac{\partial \tau_{ij}}{\partial x_j} \quad (2)$$

$$\frac{\partial}{\partial x_i} (u_i (\rho E + p)) = \frac{\partial}{\partial x_i} \left(k_{eff} \frac{\partial T}{\partial x_i} \right) \quad (3)$$

where u_i is overall velocity vector, E is the total energy, τ_{ij} is the stress tensor, and k_{eff} is the effective conductivity ($k_{eff} = k + k_t$, k_t is the turbulent thermal conductivity).

In the solid region the energy transport equation for steady state is expressed as Equation (4):

$$\frac{\partial}{\partial x_i} \left(k_{sl} \frac{\partial T}{\partial x_i} \right) = 0 \quad (4)$$

where k_{sl} is the thermal conductivity of the solid material.

To evaluate the heat transfer performance of microchannel heat sink, the average heat convection coefficient, h , is given in Equation (5), where Q_w uses the total heat transfer rate of the wall surface.

$$h = \frac{Q_w}{T_w - T_b} \quad (5)$$

The Nusselt number is defined by Equation (6):

$$Nu = \frac{h d_h}{k} \quad (6)$$

Hydraulic diameter is calculated through Equation (7):

$$d_h = \frac{4A}{C} \quad (7)$$

The total pressure drop of the fluid in the microchannel is defined as Equation (8):

$$\Delta P = P_{in} - P_{out} \quad (8)$$

where P_{in} and P_{out} use the area weighted average value obtained from the CFD results at the entrance and exit plane of the microchannel.

The pump power to drive fluid flow in microchannels, W , is calculated by Equation (9):

$$W = \frac{\dot{m}}{\rho} \Delta P \quad (9)$$

There are irreversible losses in the flow and heat transfer process of the coolant in the microchannel. The irreversible losses contain two parts: One part is the irreversible loss caused by heat transfer driven by the temperature difference, which is expressed by $\dot{S}_{g,\Delta T}$ as shown in Equation (10). Under the same heat flux, the smaller the temperature difference during the heat transfer process, the higher the average heat convection coefficient of the microchannel, and the corresponding $\dot{S}_{g,\Delta T}$ is also lower. The second part is the irreversible loss caused by the frictional flow in the microchannel, which is expressed by $\dot{S}_{g,\Delta P}$ as shown in Equation (11), and this loss is directly related to the pumping power required to drive the same mass flow fluid. In this paper, the total entropy generation rate \dot{S}_g in the heat transfer process as shown in Equation (12) is used to evaluate the comprehensive performance of the microchannel by assuming that the fluid is in a stable flow state and the temperature

change along the length of the channel is much smaller than the core temperature of the fluid [36,37].

$$\dot{S}_{g,\Delta T} = \frac{q_w A (T_w - T_b)}{T_w T_b} \quad (10)$$

$$\dot{S}_{g,\Delta P} = \frac{\dot{m}}{\rho_b T_b} \Delta P \quad (11)$$

$$\dot{S}_g = \frac{q_w A (T_w - T_b)}{T_w T_b} + \frac{\dot{m}}{\rho_b T_b} \Delta P \quad (12)$$

2.3. Mesh Description and Independence

The physical model consists of 10 flow channels. According to the principle of symmetry, one of them is intercepted for analysis. In this analysis, STAR-CCM+ was used to build polyhedral meshes with cylindrical prism layers. As shown in Figure 3, the mesh of the fluid region was finely constructed with 7 wall prism layers, making the wall $Y^+ < 1$, and the relatively coarse mesh is adopted for the solid region. The mesh sizes of 287,842, 552,704, and 764,002 were applied to conduct the mesh independence analysis.

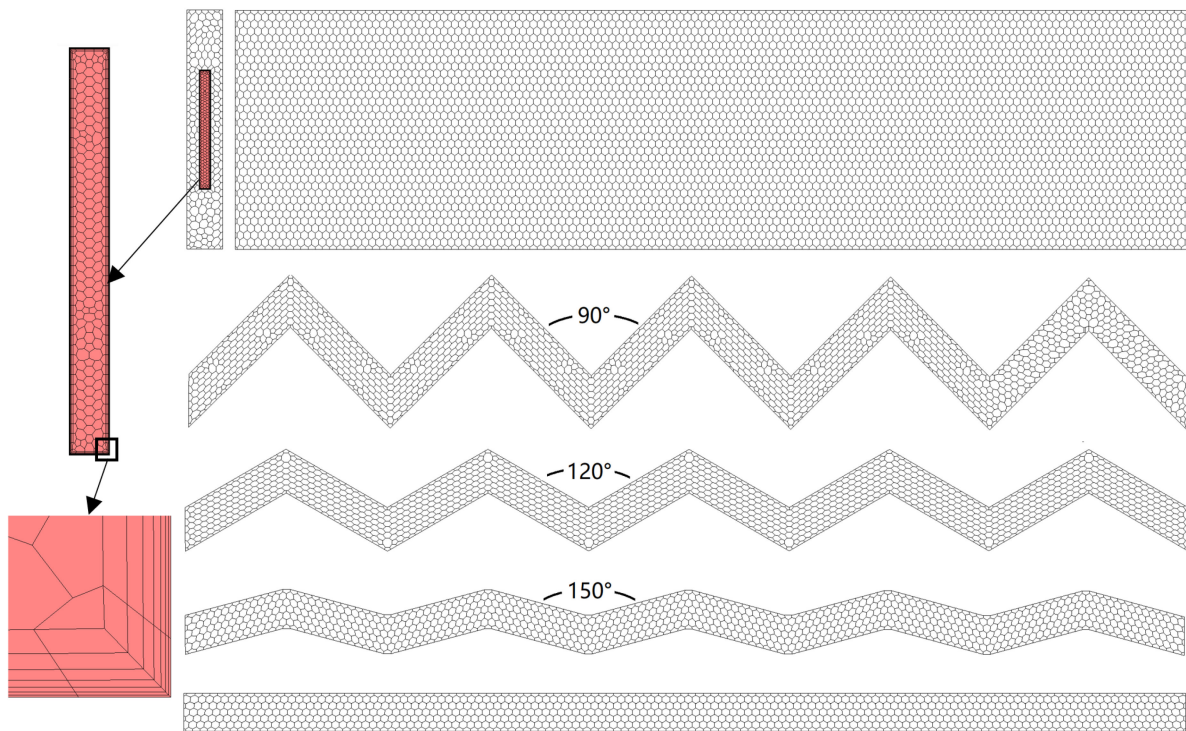


Figure 3. Mesh models.

Figure 4a,b show the comparison of ΔP and h curves for all three mesh size cases. As illustrated in this result, the error in the ΔP and h between the mesh sizes 552,704 and 764,002 is quite small. Taking into account the computational accuracy and efficiency, the rest of the study used 500,000 meshes as the baseline.

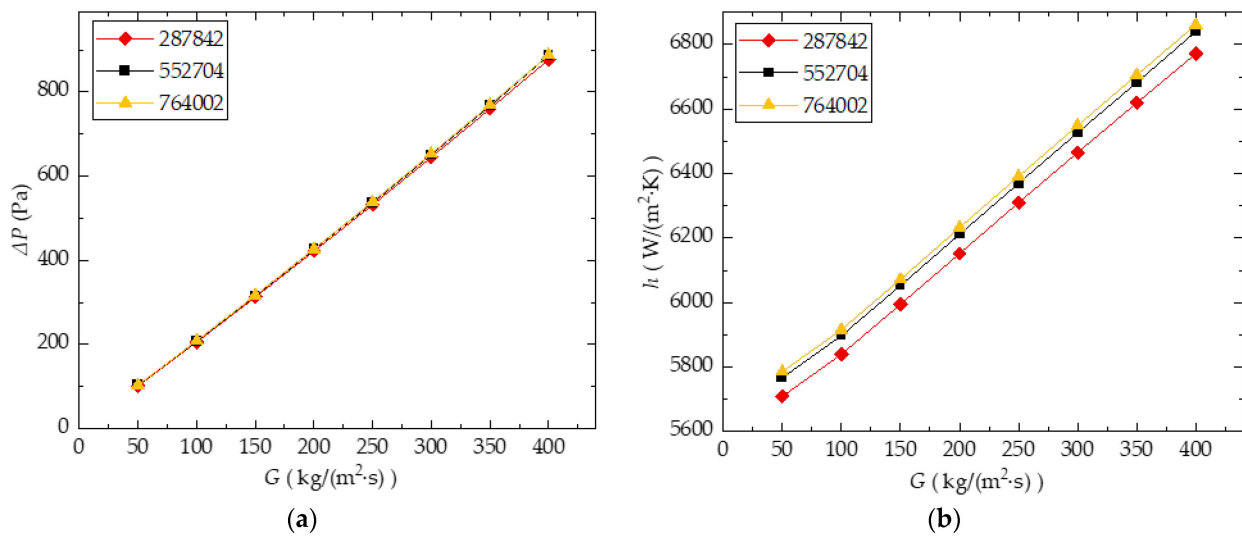


Figure 4. Mesh independent analysis result: (a) ΔP ; (b) h .

2.4. Validation

To further validate the feasibility of the numerical method, in this study, the numerical results with the SST k- ω and k- ϵ turbulent models are compared with the test data obtained in [38]. The comparison was conducted under water-cooled condition with an Re range of 500~3500 (sCO₂ as a coolant is detailed in [39]). The comparison result in Figure 5 shows that the numerical result maintained consistency with the experiment data well in the linear flow state when $Re < 1500$. When $Re > 2000$, compared with the k- ϵ turbulence model (with maximum relative error 33.8%), the calculation result of the k- ω turbulent model of shear stress transfer (with maximum relative error 13.7%) shows a better consistency with the experiment data. In the transitional region from laminar to turbulent flow, $1500 < Re < 2000$, the maximum relative error is 26.5% using laminar models. Since the maximum Reynolds numbers of analysis cases in the following study can reach more than 5000, the k- ω SST model will be adopted for turbulent flow cases.

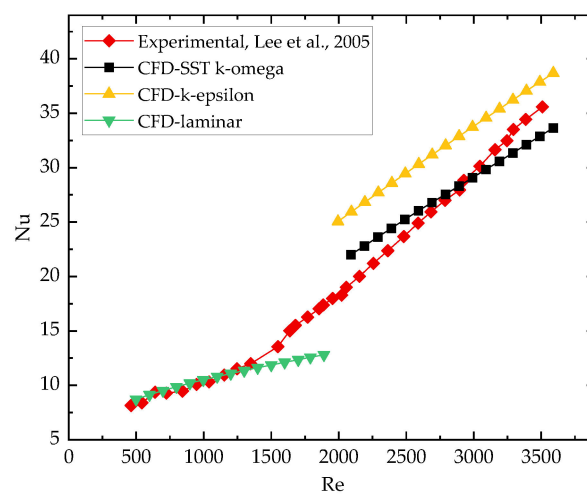


Figure 5. Validation with experimental data [38].

3. Results and Discussions

By comparing the thermophysical properties of water and sCO₂, it is apparent that the thermal conductivity of CO₂ is lower than that of water by no more than one order

of magnitude. Nevertheless, the specific heat capacity of sCO₂ shows several orders of magnitude higher than that of water, which is beneficial for its heat transfer performance in microchannels. The dynamic viscosity of sCO₂ is also lower than that of water by several orders of magnitude, which is significantly beneficial for its flow characteristics in microchannels. In this analysis, the thermal and hydraulic characteristics of water and sCO₂ in straight and zigzag microchannels are compared and analyzed to understand the feasibility of replacing water with sCO₂ as a coolant.

3.1. Comparative Study of Straight Channel Cases in Different Mass Flux

In this section, a comparative study is conducted on the following four parameters, ΔP , h , T_{hsurr} , and \dot{S}_g , to analyze the thermal and hydraulic performance of water and sCO₂ in microchannels. Six inlet temperatures of 306 K, 307 K, 308 K, 310 K, 315 K, and 320 K are used for the analysis of CO₂. For liquid water, the inlet temperature is 308 K. The inlet mass flux range of the two coolants is 50~1000 kg/(m²·s). All cases adopt the pressure outlet boundary. The outlet pressure is 8 MPa for CO₂-cooled cases and 0.1 MPa for water-cooled cases. The constant heat flux between 4 and 120 W/cm was adopted for the heat surface of the microchannel.

3.1.1. Pressure Drop

It is obvious as illustrated in Figure 6 that the ΔP curve of the water-cooled microchannel is significantly higher than that of the CO₂-cooled microchannel at each inlet temperature. Obviously, this is in line with our predictions. This is because the dynamic viscosity of water at room temperature is significantly higher than that of sCO₂ with its condition close to the pseudocritical state. For sCO₂-cooled cases in this comparison analysis, the channel ΔP increases with increasing T_{in} . This is because the ΔP through the microchannel is influenced by the dynamic viscosity and density of the coolant. These two thermophysical parameters both decrease with increasing T_b , but the influence of density change takes the lead.

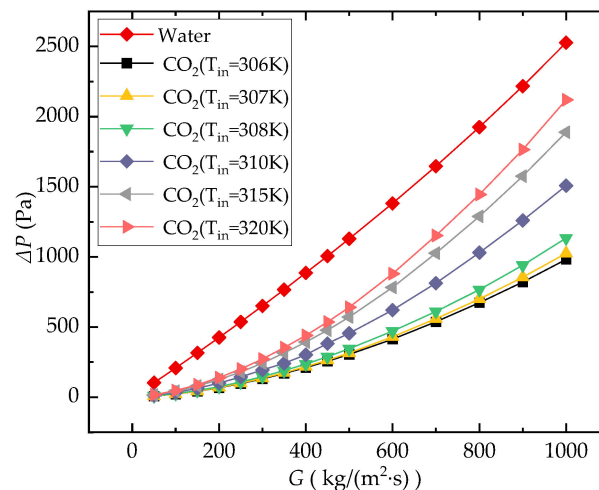


Figure 6. Comparison of ΔP of the microchannel ($q_w = 40,000 \text{ W/m}^2$).

The pressure drop of the water-cooled channel is almost linear with the change in G , while this does not happen for the CO₂-cooled one. This is also because the density and dynamic viscosity of CO₂ change drastically with temperature near the pseudocritical point, especially density, which is much more sensitive to the temperature compared to the water. Similar conclusions also appeared in [30].

3.1.2. Average Heat Convection Coefficient

As illustrated in Figure 7, h of the water-cooled cases is higher than those of sCO₂-cooled cases with low mass flux (<250 kg/(m²·s)). This is because the bulk temperature T_b of the fluid increases significantly relative to T_{in} at low mass flow, resulting in a large deviation in T_b from the pseudocritical temperature ($T_m = 307.75$ K at 8 MPa) for CO₂. This will lead to a sharp deterioration in the thermophysical (thermal conductivity and specific heat) properties of CO₂. As the contour diagram in Figure 8 shows, the temperature change in the fluid along the channel decreases with the increase in G . Figure 7 also shows that h of water and CO₂ both gradually increase with the increasing G , but the growth rate of the CO₂-cooled case is larger. As G increases, the temperature variation of the CO₂ fluid along the flow path becomes smaller, making its deviation from the pseudocritical point smaller. In this high mass flux condition, the h for water-cooled channels is not as good as h for the CO₂-cooled channels in the cases where the T_{in} is close to T_m ($T_{in} = 306$ K, 307 K, 308 K, 310 K). For CO₂-cooled cases, the highest value, and the highest rate of increase in h , occur at $T_{in} = 308$ K, which is closest to T_m . This is because the closer the state of CO₂ is to the pseudocritical point, the better its thermophysical properties, and the more intense the change in its thermophysical properties.

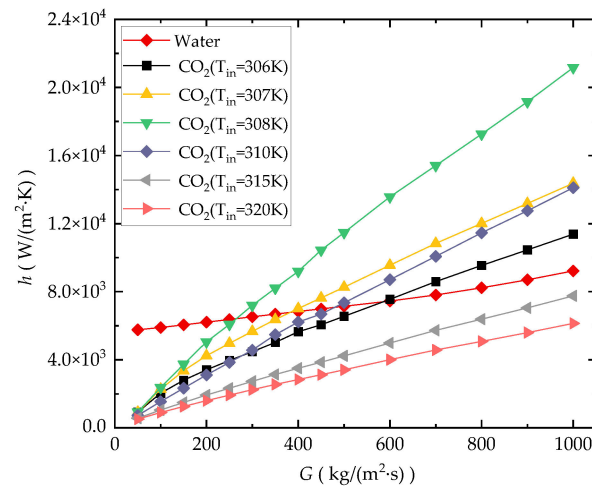


Figure 7. Comparison of h of the microchannel ($q_w = 40,000$ W/m²).

3.1.3. Average Temperature of the Heated Wall

Figure 9 shows the comparison result of the average temperature of the heated wall T_{hsur} of the CO₂-cooled and water-cooled microchannels. In this analysis, $T_{in} = 308$ K, $q_w = 40,000$ W/m², $P_{out} = 8$ MPa for the sCO₂ case, $P_{out} = 0.1$ MPa for the water case, and $G = 50$ – 500 kg/(m²·s). It also shows that the T_{hsur} of the water-cooled channel is lower than that of the CO₂-cooled channel only at an extremely low mass flux. This is also caused by the large deviation in the temperature of the CO₂ fluid from T_m under low mass flux conditions, resulting in the deterioration of its thermophysical properties and the weakening of the heat transfer performance. This impact will gradually decrease with increasing mass flux. When $G > 100$ kg/(m²·s), T_{hsur} of the CO₂-cooled channel will be lower than that of the water-cooled channel. When $G > 300$ kg/(m²·s), the average temperature difference in the heated surface between the two coolant-based cooling cases tends to be stable, and values of T_{hsur} of the CO₂-cooled channel are 0.5–0.7 K lower than those of the water-cooled channel.

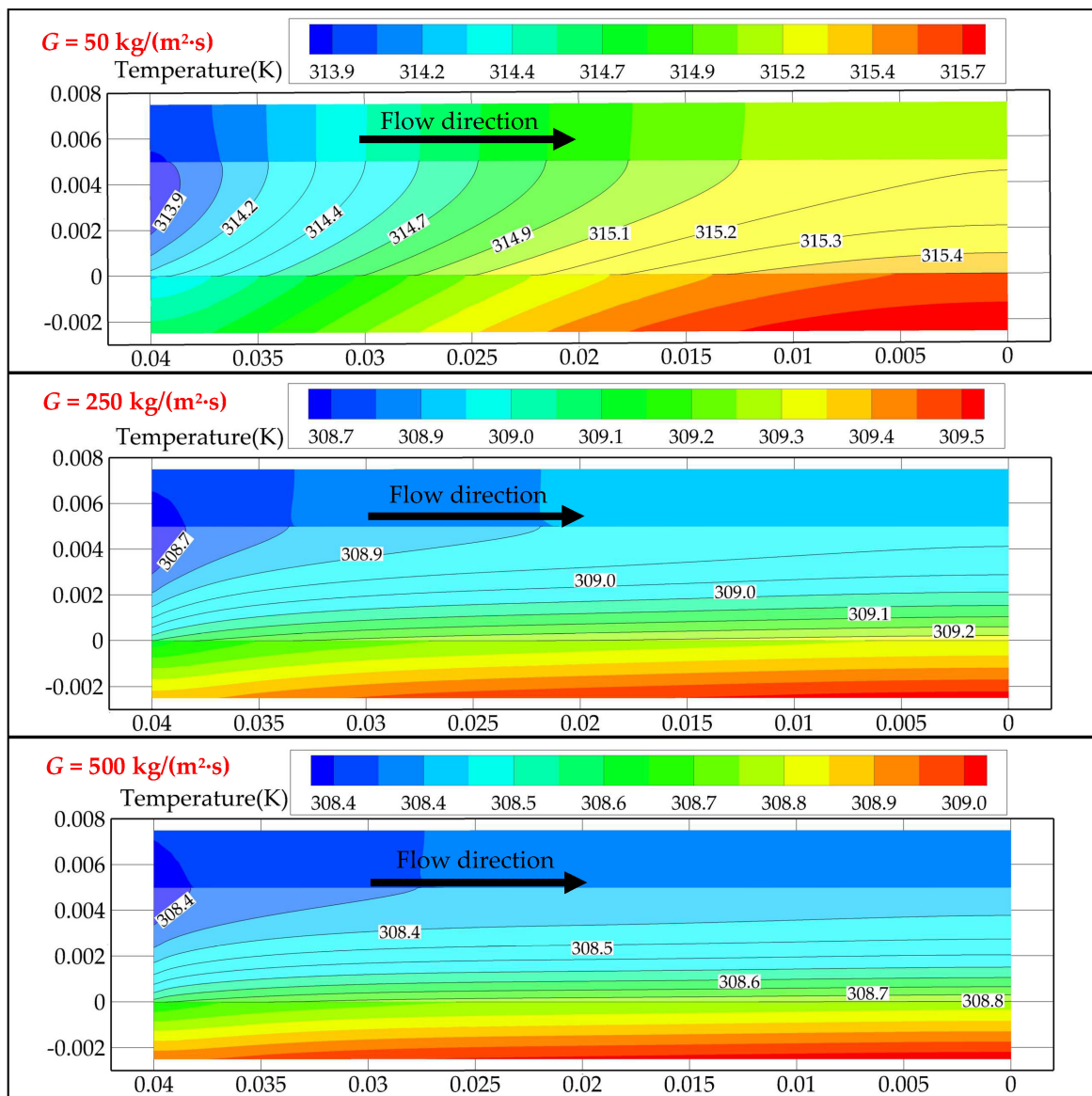


Figure 8. Changes in channel temperature along the flow direction.

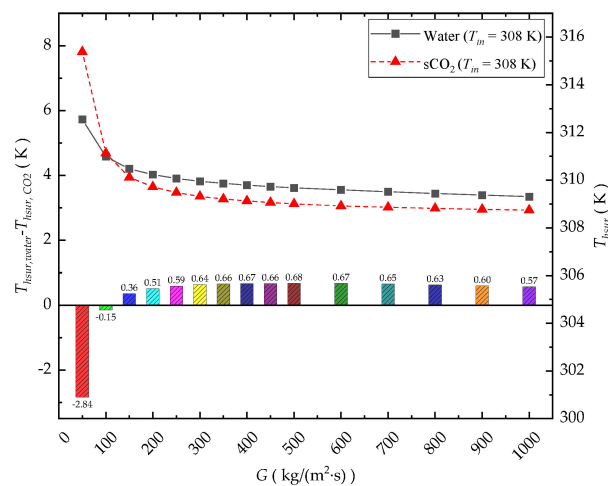


Figure 9. Comparison of T_{hsur} of the microchannel.

3.1.4. Entropy Generation Rate

Figure 10a,b shows the comparison of entropy generation rate \dot{S}_g under different boundary conditions with water and CO₂ as coolants at mass flux between 50~1000 kg/(m²·s) against different inlet temperatures (CO₂: 306 K, 307 K, 308 K, 310 K, 315 K, 320 K; water: 308 K).

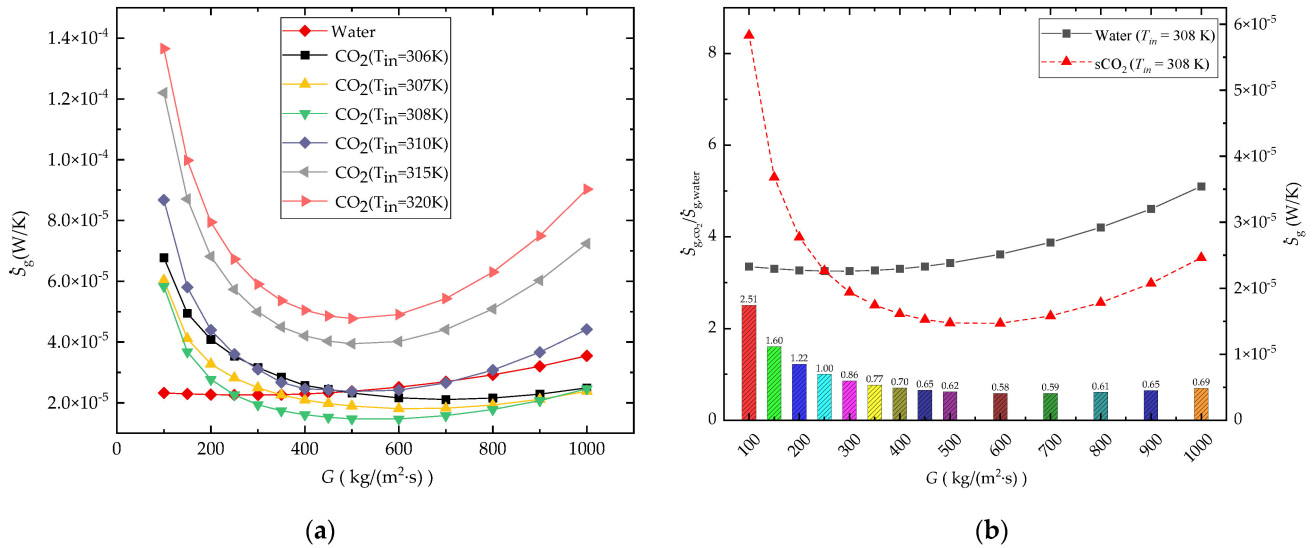


Figure 10. Comparison results of the entropy generation rate in different G : (a) \dot{S}_g ; (b) $S_{g,CO_2} / S_{g,water}$.

As shown in Figure 10a, the \dot{S}_g of the CO₂-cooled microchannel is lower than that of the water-cooled microchannel at relatively large mass flux in the case of $T_{in} = 306$ K, 307 K, and 308 K, and the lowest \dot{S}_g curve occurs when $T_{in} = 308$ K. For the cases with $T_{in} = 315$ K and 320 K, the \dot{S}_g of the CO₂-cooled microchannel is higher than that of the water-cooled microchannel due to the large deviation from the pseudocritical point. It also means that the comprehensive performance of the microchannels can be improved on the basis of maintaining the state of CO₂ close to the pseudocritical point.

The ratio value of S_{g,CO_2} at $T_{in} = 308$ K to $\dot{S}_{g,water}$ in Figure 10b also shows that under the current working condition, when $G < 250$ kg/(m²·s) the performance of the CO₂-cooled channel is not as good as that of the water-cooled channel, and when $G > 500$ kg/(m²·s) using sCO₂ as a coolant can decrease the \dot{S}_g to 0.58~0.69 times of the water-cooled straight microchannel.

It can also be seen from Figure 10a that there are minimum-value entropy generation rates for all water-cooled and sCO₂-cooled cases within the current analyzed mass flux range. This is because as the mass flux increases, as shown in Figure 11a,b, for both the water-cooled and CO₂-cooled channels, the $\dot{S}_{g,\Delta T}$ shows a decreasing trend due to the increasing heat convection coefficient in the microchannel, and $\dot{S}_{g,\Delta P}$ shows a increasing trend due to the increasing channel pressure drop. The total entropy generation rates \dot{S}_g for both water-cooled and CO₂-cooled cases decrease first, then increase continuously with the increasing G .

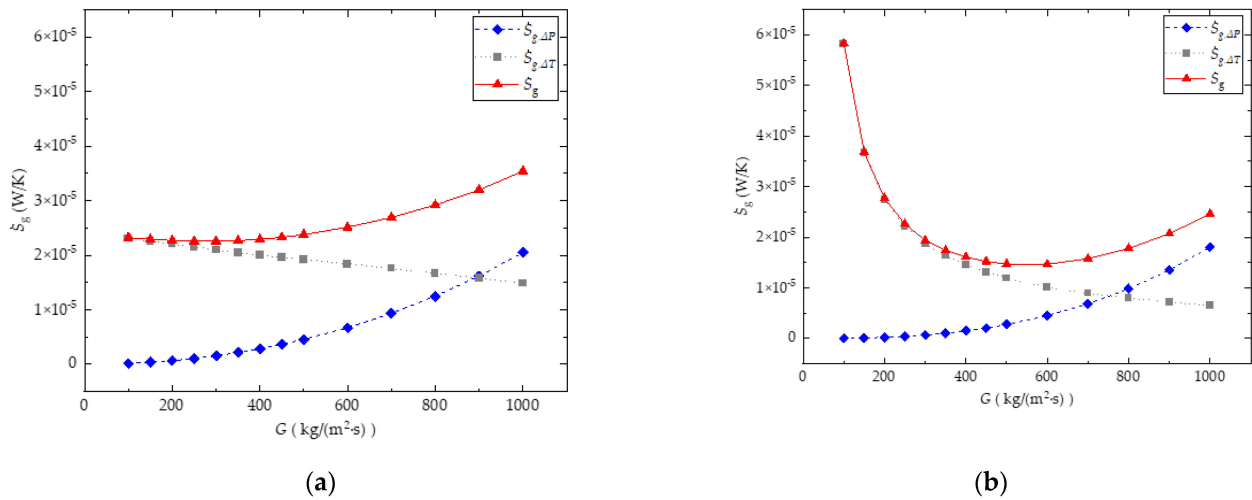


Figure 11. Effect of G on $\dot{S}_{g,\Delta P}$, $\dot{S}_{g,\Delta T}$, and \dot{S}_g : (a) water-cooled channel ($T_{in} = 308$ K, $P_{out} = 0.1$ MPa); (b) CO₂-cooled channel ($T_{in} = 308$ K, $P_{out} = 8$ MPa).

3.2. Comparative Study of Straight-Channel Cases in Different Heat Flux

It can be seen from the analysis in Section 3.1 that in order to ensure excellent heat transfer characteristics of the CO₂ coolant, it is essential to maintain the CO₂ state close to the pseudocritical point. With the increase in q_w , the temperature change in the fluid along the channel will increase, causing the fluid state to deviate more from the pseudocritical point. This section studies the effect of heat flux (q_w) on the h , ΔP , and \dot{S}_g of straight microchannels cooled by water and CO₂ for three different mass fluxes (500, 1000, 1500 kg/(m²·s)) at $T_{in} = 308$ K, $P_{out} = 8$ MPa for the sCO₂ case, and $P_{out} = 0.1$ MPa for the water case.

3.2.1. Average Heat Convection Coefficient

Figure 12 shows the effect of q_w on heat transfer performance for both water-cooled and CO₂-cooled channels. It can be seen from the result that the change in q_w has little impact on h for water-cooled cases. This is because the change in coolant T_b caused by the increase in q_w has little effect on the thermophysical properties (specific heat and thermal conductivity) of the water. For the sCO₂ coolant, however, as $T_{in} = 308$ K, the fluid state is near the peak position of the curves of thermal conductivity and specific heat capacity. At this position, the values of both thermal conductivity and specific heat capacity decrease dramatically as temperature deviates from the T_m (307.75 K at 8 MPa). When q_w continuously increases at a fixed mass flux, the deviation in T_b from T_{in} will increase, and the thermophysical properties of CO₂ will deteriorate. As a result, the h of the CO₂-cooled channel decreases rapidly with the increase in q_w .

3.2.2. Pressure Drop and Pumping Power

Figure 13a,b illustrate the effect of q_w on channel pressure drop (ΔP) and pump power consumption (W), respectively. As shown in Figure 13a, the ΔP of the water-cooled channel is significantly higher than that of the CO₂-cooled channel. This result also shows that the variation in q_w has little impact on the channel pressure drop in water-cooled cases. However, for the CO₂-cooled channel, the ΔP curves show a slight upward trend as q_w increases. This is caused by the increase in T_b of CO₂, which will lead to a decrease in the density and dynamic viscosity of CO₂. The influence of these two parameters on the channel ΔP is opposite and the combined effect is that the ΔP of the CO₂-cooled channel increases slightly with increasing q_w . Although the ΔP in the water-cooled channel is higher, the difference in pump power consumption between the CO₂-cooled and water-cooled

channels is relatively small under the same mass flux, as shown in Figure 13b, because of the lower density of the CO₂ compared to water.

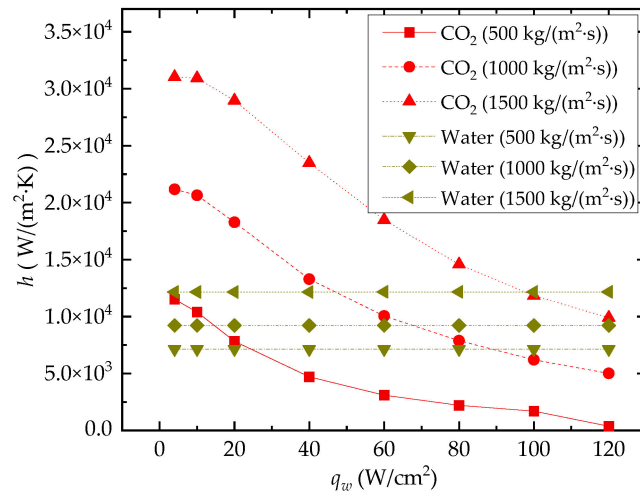


Figure 12. Effect of q_w on h ($T_{in} = 308$ K).

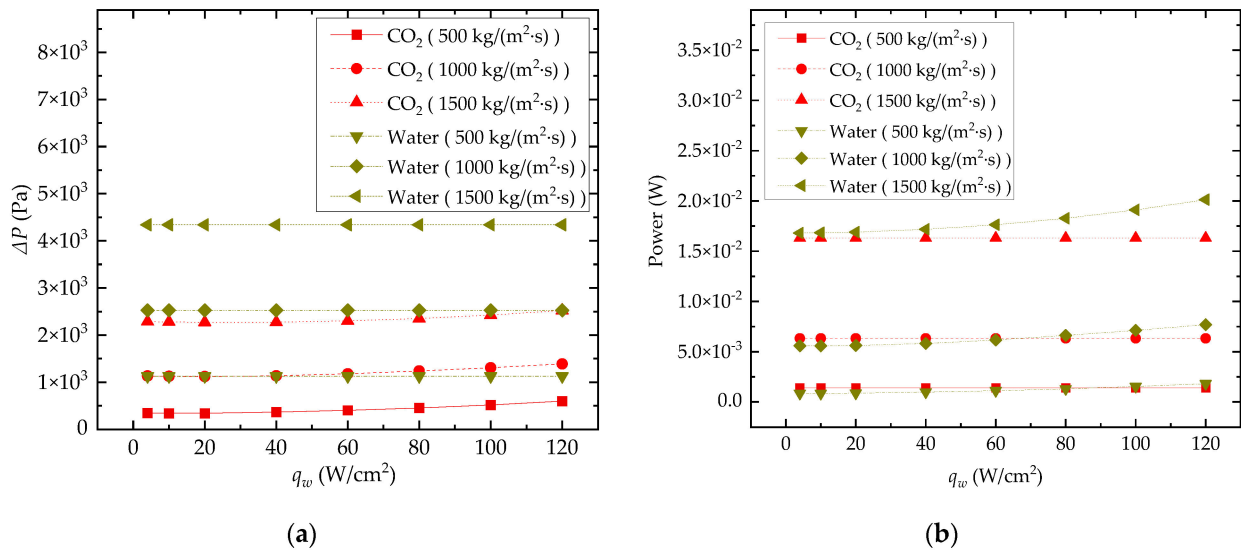


Figure 13. Effect of q_w on ΔP and pumping power consumption: (a) pressure drop; (b) power.

3.2.3. Entropy Generation Rate

The effect of q_w on entropy generation rate \dot{S}_g is presented in Figure 14. It can be seen from the comparison result that with the increase in heat flux density, the \dot{S}_g of both the water-cooled channel and the CO₂-cooled channel show an upward trend, but the increase rate of the CO₂-cooled channel is higher. This means that the irreversible loss of the CO₂-cooled channel is more affected by the heat flux. It can also be seen from the comparison of the curves that the accelerating upward trend of \dot{S}_g with the increase in q_w for the CO₂-cooled microchannel is more significant. This is because an increase in q_w leads to a greater deviation from the pseudocritical point of the CO₂ fluid state, which will also weaken the heat transfer performance of the channel.

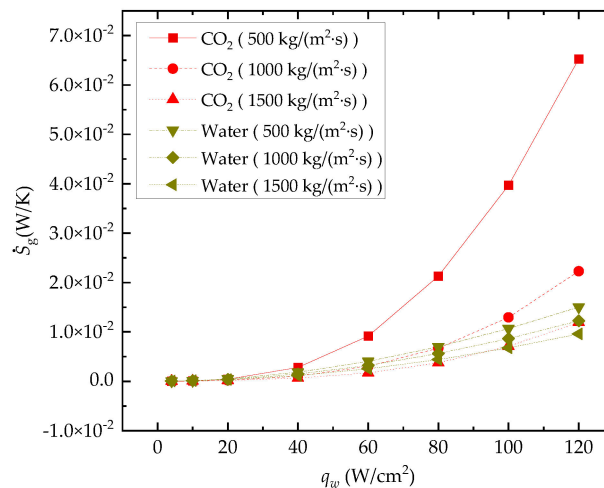


Figure 14. Effect of heat flux on \dot{S}_g .

3.3. Comparative Analysis of Zigzag Channels

Zigzag is a common channel type in industrial applications. The existence of bends along the channel can increase the intensity of the turbulence of the fluid and enhance the mixing of the wall fluid and the mainstream, to achieve the purpose of strengthening heat transfer. In this analysis, 90° , 120° , 150° , and 180° (straight channel) were used for the comparative study to investigate the heat transfer enhancement characteristic for zigzag channels cooled by water and CO_2 . In this comparative analysis, four inlet temperatures ($T_{in} = 308, 310, 315$, and 320 K) and a fixed outlet pressure of $P_{out} = 8$ MPa are considered for the CO_2 -cooled channel. For the water-cooled microchannel cases, fixed $T_{in} = 308$ K and $P_{out} = 0.1$ MPa are used, and $G = 50\sim 500$ kg/($\text{m}^2\cdot\text{s}$) and $q_w = 40,000$ W/ m^2 are set for both water-cooled and CO_2 -cooled cases.

3.3.1. Comparative Study of h under Different Angles of Bend in The Zigzag Channel

Figure 15a–d show the comparison of the h in CO_2 -cooled and water-cooled channels with four different bending angles, including the straight channel ($\theta = 180^\circ$). The h of the water-cooled channel for all four bending angle channel types is greater compared to the CO_2 -cooled channel under low mass flux. This means that the heat transfer performance of CO_2 is worse than that of water at a relatively low mass flux. This is because the lower mass flux will aggravate the deviation in the T_b and T_w from the T_{in} of the CO_2 fluid, resulting in a greater deviation in the state of CO_2 from the pseudocritical point. The thermophysical parameters (specific heat and thermal conductivity) of CO_2 are greatly reduced.

However, the increased rate of h with G of the CO_2 -cooled channel is higher than that of the water-cooled channel for all four bending angle channel types. This result means that the increase in mass flux has a greater impact on h of the CO_2 -cooled channel than on the water-cooled one. This is because increasing the mass flux not only increases the Re of the microchannel and enhances turbulence, but also makes the T_b of CO_2 closer to T_m , and the heat transfer performance can be further improved.

Figure 16a,b provide the comparison of h in different bend angle cases for CO_2 -cooled and water-cooled microchannels of zigzag type, respectively. Obviously, the comparison results in these figures indicate that for both CO_2 -cooled and water-cooled microchannels, reducing the turning angle is conducive to enhancing heat transfer. However, the comparison result also shows that the existence of bends has a more significant impact on the water-cooled channel. Compared to the straight channel case, the h of the zigzag channel with $\theta = 150^\circ$ increases significantly. However, the improvement in heat transfer performance of water-cooled cases by further reducing θ is no longer as significant as the transition from straight to zigzag type.

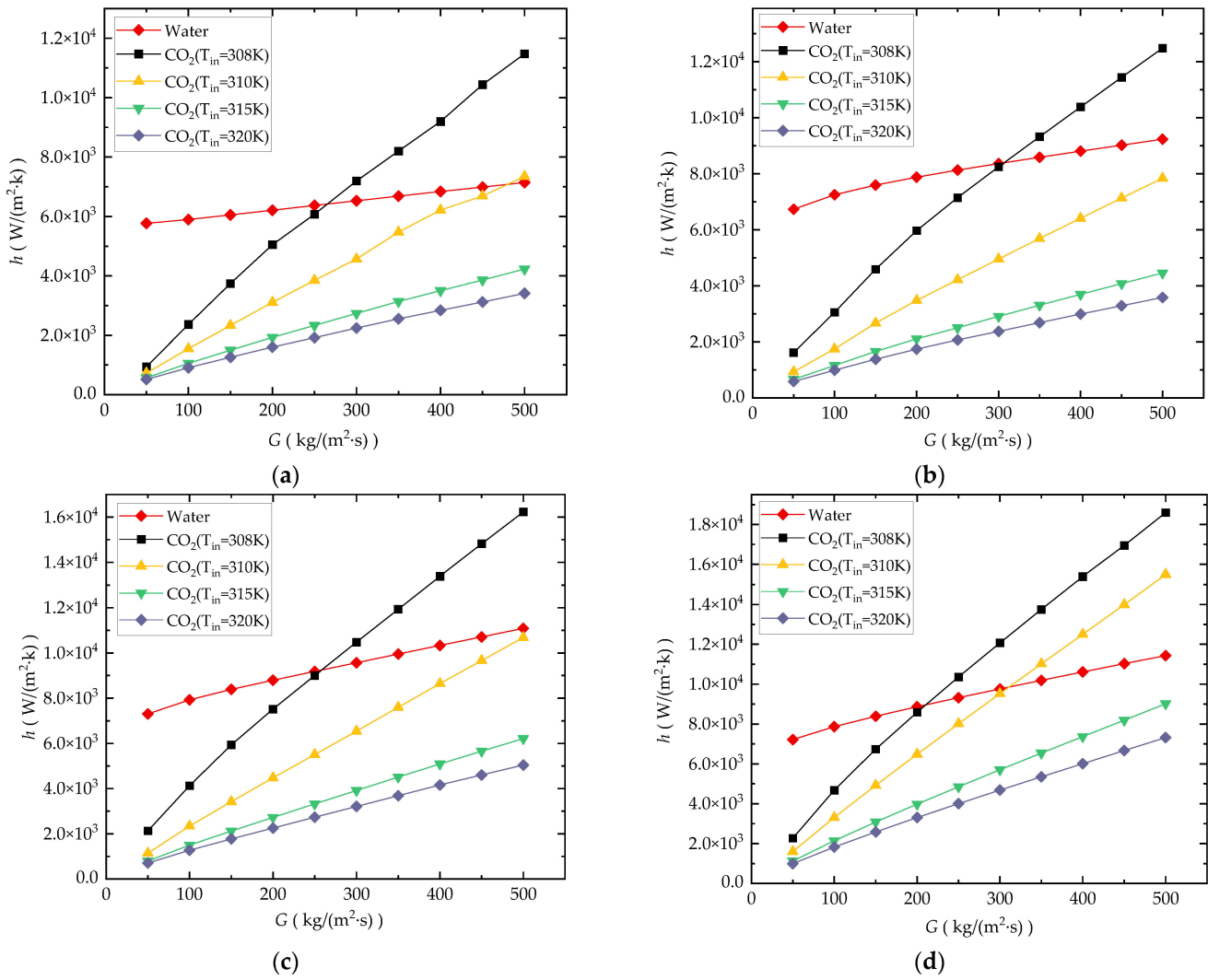


Figure 15. Comparison of h : (a) straight channel; (b) $\theta = 150^\circ$; (c) $\theta = 120^\circ$; (d) $\theta = 90^\circ$.

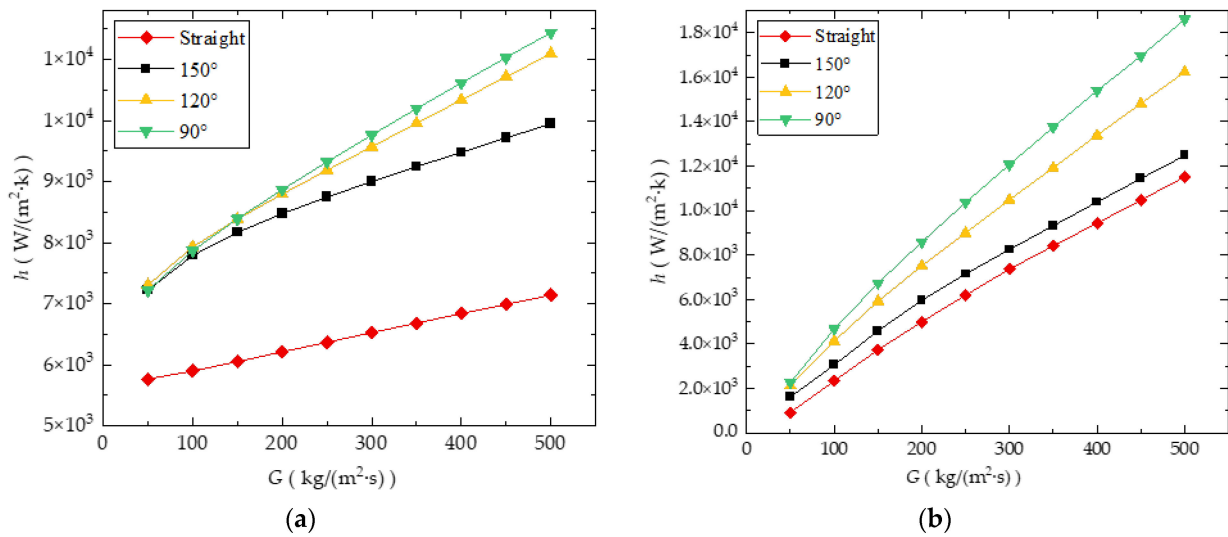


Figure 16. Comparison of the effect of bend angle on h : (a) water-cooled channel; (b) CO₂-cooled channel (T_{in} = 308 K).

In the analysis cases, the fluid of the water-cooled channel is in a laminar state with low Re (6.17~61.7), and the existence of bends in the zigzag channel can greatly improve the intensity of turbulence and significantly thin the thermal boundary layer compared to the straight channel, as illustrated in Figure 17a,b. For the CO₂-cooled channel, the heat transfer enhancement effect produced by using a zigzag channel instead of the straight channel is not as great as that of the water-cooled channel. This is because the sCO₂-cooled straight channel has a thinner thermal boundary layer than the water-cooled straight channel, as illustrated in Figure 17c,d, and the variation in the thickness of the thermal boundary layer caused by the bending in the channel is not as significant as that of the water-cooled channel.

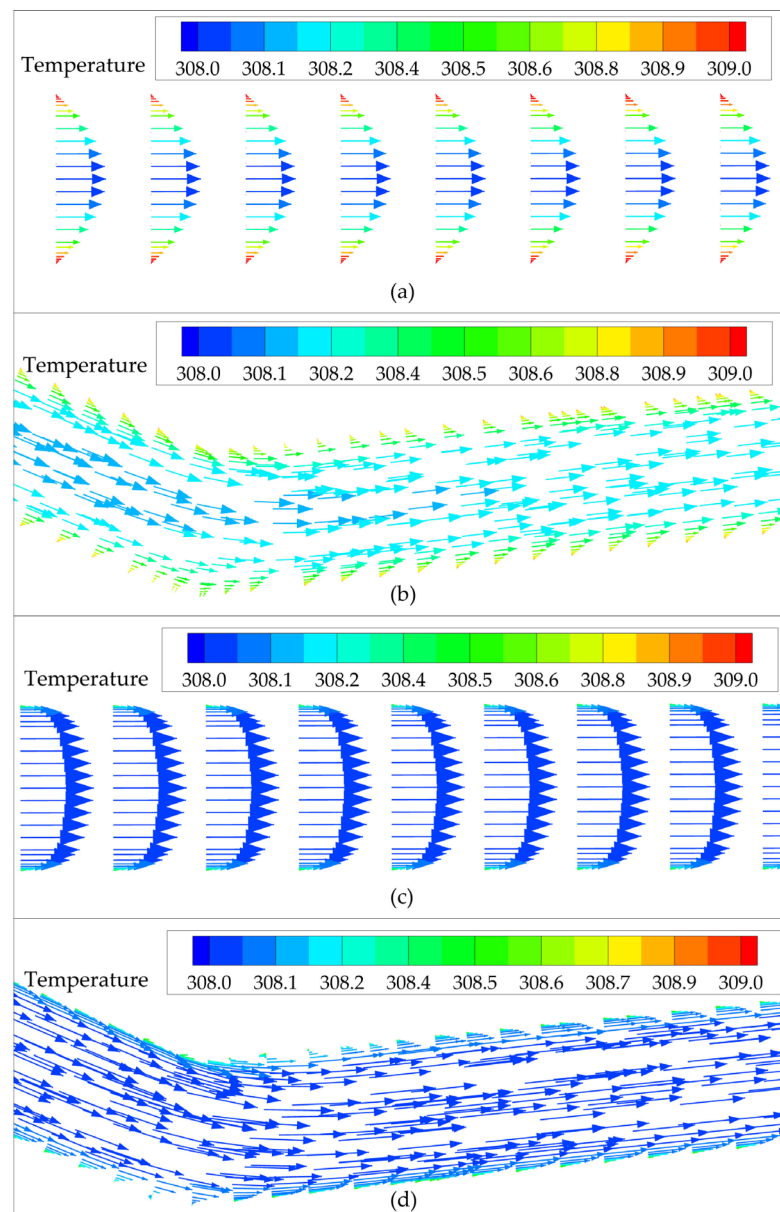


Figure 17. Velocity vector diagram of the cross section of microchannel ($G = 500 \text{ kg}/(\text{m}^2 \cdot \text{s})$, $T_{in} = 308 \text{ K}$): (a) water-cooled straight channel; (b) water-cooled zigzag channel ($\theta = 150^\circ$); (c) CO₂-cooled straight channel; (d) CO₂-cooled zigzag channel ($\theta = 150^\circ$).

3.3.2. Comparative Study of \dot{S}_g under Different Angles of Bend in the Zigzag Channel

The existence of and reduction in the bend angle of the zigzag channel can enhance thermal performance, but cause an increase in the channel pressure drop, which leads to an increase in pump power consumption. This means that the thermal entropy generation decreases while the flow entropy generation increases. The total entropy generation rate \dot{S}_g is illustrated in Figure 18a–d for the water-cooled and sCO₂-cooled microchannel in different θ cases.

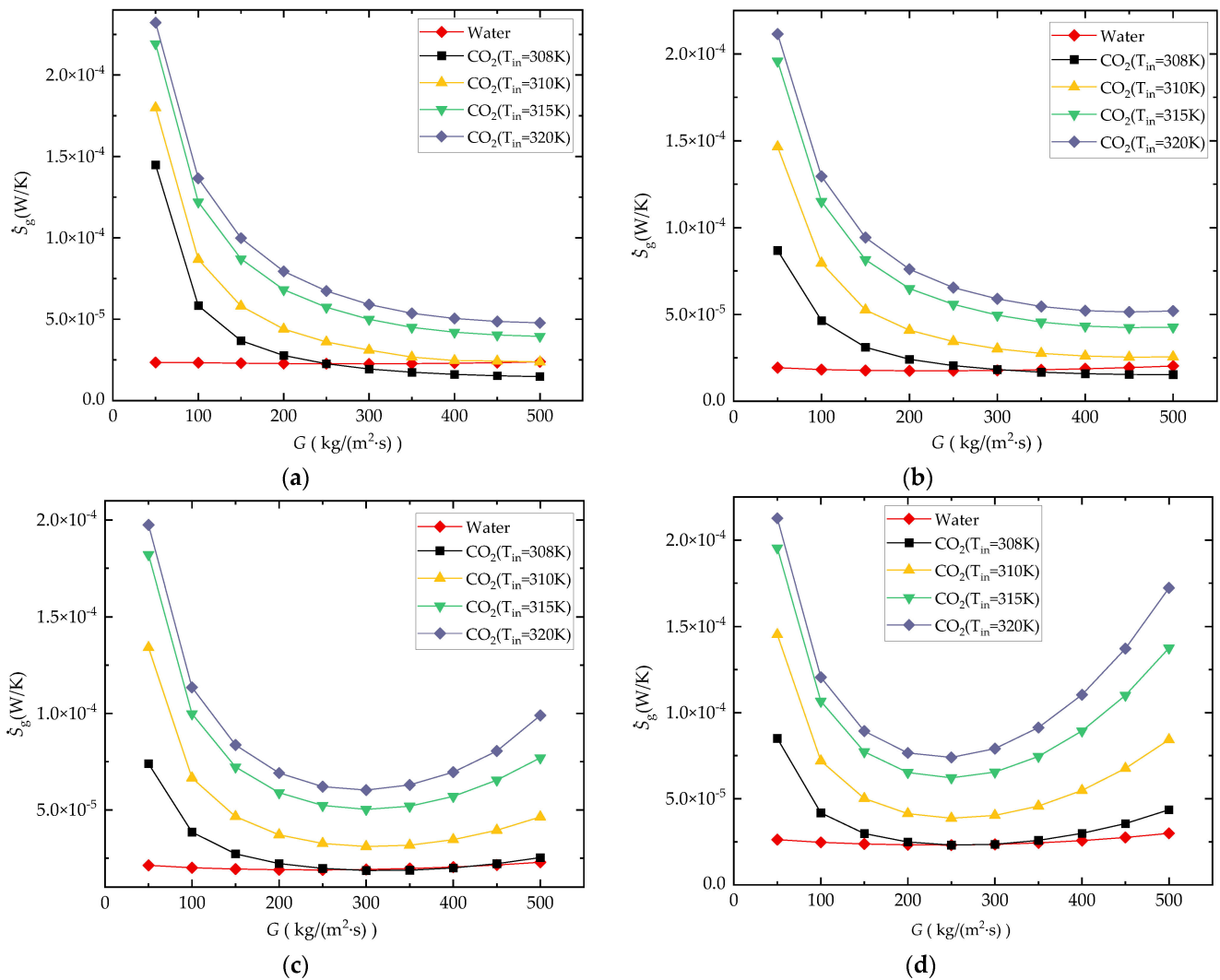


Figure 18. Comparison of \dot{S}_g : (a) straight channel; (b) $\theta = 150^\circ$; (c) $\theta = 120^\circ$; (d) $\theta = 90^\circ$.

For the CO₂-cooled microchannel of straight type and zigzag type with $\theta = 150^\circ$, as shown in Figure 18a,b, the \dot{S}_g shows a decreased trend as G increases from 50 to 500 kg/(m²·s), which means that the decreasing amplitude of thermal entropy generation caused by the increasing flow flux is greater than the increasing amplitude of flow entropy generation. For the CO₂-cooled microchannel of zigzag type with $\theta = 120^\circ$ and $\theta = 90^\circ$, as shown in Figure 18c,d, the \dot{S}_g curve presents a U shape. The minimum value of \dot{S}_g occurs when G is between 250 and 300 kg/(m²·s). With the decrease in θ of the zigzag microchannel, the proportion of the flow entropy generation in total entropy generation becomes larger. Figure 18 also shows that when $T_{in} = 310, 315,$ and 320 K, \dot{S}_g of the CO₂-cooled case is larger than that of the water-cooled case in the whole analysis flow flux range for all straight and zigzag microchannels. In this case, there is no advantage in using CO₂

to replace water as a coolant. When $T_{in} = 308$ for straight type and zigzag type with $\theta = 150^\circ$, the \dot{S}_g of the CO₂-cooled microchannel is lower than that of the water-cooled channel under high-flow flux conditions.

Figure 19a,b show the effect of θ on \dot{S}_g of the water-cooled and sCO₂-cooled microchannel with $T_{in} = 308$ K, respectively. It can be seen from the analysis result that in water-cooled cases, the zigzag channel with $\theta = 150^\circ$ has the best comprehensive performance (lowest value of \dot{S}_g), followed by $\theta = 120^\circ$ and straight channels, and the zigzag channel with $\theta = 90^\circ$ is the worst. For the cases of sCO₂-cooled channels, the \dot{S}_g of the straight channel and zigzag channel with $\theta = 150^\circ$ is better, and with a reduction in the value of θ , the \dot{S}_g of the zigzag channel gradually increases. This analysis result also shows that although the existence of bends in the microchannel can improve the h of the sCO₂-cooled microchannel, it is not beneficial to its comprehensive performance evaluated by \dot{S}_g . However, the existence of obtuse bends in the channel can improve the comprehensive performance to some extent for the water-cooled microchannel.

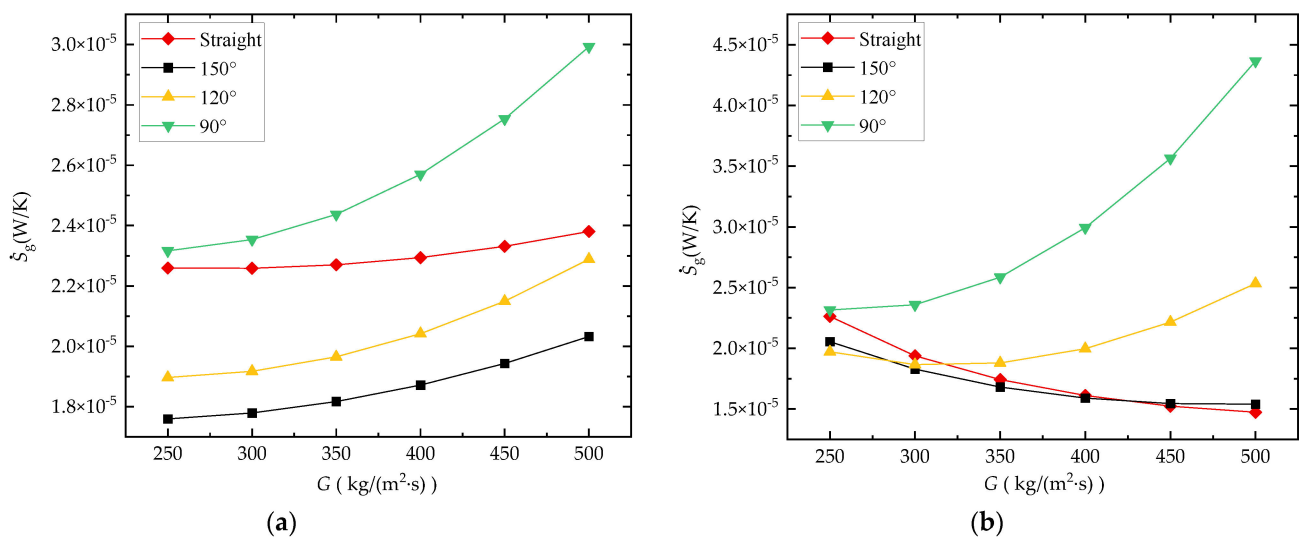


Figure 19. Comparison of the effect of bend angle on \dot{S}_g : (a) channel cooled by water; (b) channel cooled by CO₂ ($T_{in} = 308$ K at $P_{out} = 8$ MPa).

4. Conclusions

A numerical comparative study was carried out for sCO₂-cooled and water-cooled straight and zigzag ($\theta = 90^\circ, 120^\circ$, and 150°) microchannels. The mass flux (G) ranges from 50 to 1000 kg/(m²·s) and the heat flux (q_w) ranges from 40,000 to 120,000 W/m² for both coolant-based cooling cases. The inlet temperature (T_{in}) for CO₂-cooled microchannels ranges from 306 K to 320 K with the operating pressure 8 MPa, which covers the pseudocritical point. The inlet temperature of the water-cooled microchannel is 308 K with the operating pressure 0.1 MPa. The following conclusions were obtained:

(1) Using sCO₂ has advantages over water in thermal and hydraulic performance in microchannels due to its excellent thermophysical properties nearby the pseudocritical point. Taking sCO₂ as a coolant makes it possible to reduce the average temperature of the heating surface (T_{hsur}) to 0.5~0.7 K and enhance the heat transfer performance in contrast to water. The entropy generation rate (\dot{S}_g) of the straight microchannel cooled with sCO₂ can reach 0.58~0.69 times the one cooled with water.

(2) Using CO₂ replacing water as the coolant can improve microchannel thermal and hydraulic performance, but the premise lies in adopting a reasonable inlet temperature, working pressure, and adequate channel mass flux according to the heat load to keep the CO₂ state near the pseudocritical point.

(3) In comparison with straight channels, zigzag channels can enhance heat transfer, but this will also increase the channel flow resistance. As for the water-cooled case, the zigzag channel with $\theta = 150^\circ$ had the best comprehensive performance represented by \dot{S}_g , while for the sCO₂-cooled case, the straight channel had the best comprehensive performance.

Author Contributions: Conceptualization, Y.T.; methodology, Y.T.; software, Y.T.; validation, Y.Z.; formal analysis, Y.T.; investigation, Y.T.; resources, Y.T.; data curation, Y.Z.; writing—original draft preparation, Y.T.; writing—review and editing, Y.Z.; visualization, Y.T.; supervision, Y.T.; project administration, Y.T.; funding acquisition, Y.T. All authors have read and agreed to the published version of the manuscript.

Funding: This research was funded by Hunan Province Education Department, China, grant number 21B0618 and Hunan Province Natural Science Project, China, grant number 2020JJ5393.

Institutional Review Board Statement: Not applicable.

Informed Consent Statement: Not applicable.

Data Availability Statement: Not applicable.

Conflicts of Interest: The authors declare no conflict of interest.

Nomenclature

A	area (m ²)	Greek symbols	
C	wet circumference (m)	ρ	density (kg/m ³)
d_h	hydraulic diameter (m)	μ	dynamic viscosity (Pa·s)
\vec{g}	gravity vector (m/s ²)	θ	bend angle
G	mass flux (kg/(m ² ·s))	Subscripts	
h	average heat convection coefficient (W/(m ² ·K))	b	bulk
k	thermal conductivity (W/(m·K))	eff	effective
\dot{m}	mass flow rate (kg/s)	$hsur$	heated surface
Nu	Nusselt number	in	inlet
P	pressure (Pa)	m	pseudocritical point
ΔP	pressure difference (Pa)	out	outlet
q	heat flux (W/m ²)	t	turbulent
Q	heat (W)	w	wall
Re	Reynolds number		
\dot{S}_g	entropy generation rate (W/K)		
T	temperature (K)		
\vec{v}	velocity vector (m/s)		

References

- Xu, L.; Yang, T.; Sun, Y.; Xi, L.; Gao, J.; Li, Y.; Li, J. Flow and Heat Transfer Characteristics of a Swirling Impinging Jet Issuing from a Threaded Nozzle. *Case Stud. Therm. Eng.* **2021**, *25*, 100970. [[CrossRef](#)]
- Deng, Z.; Shen, J.; Dai, W.; Li, K.; Song, Q.; Gong, W.; Dong, X.; Gong, M. Experimental Study on Cooling of High-Power Laser Diode Arrays Using Hybrid Microchannel and Slot Jet Array Heat Sink. *Appl. Therm. Eng.* **2019**, *162*, 114242. [[CrossRef](#)]
- Li, Y.; Guo, H.; Qi, F.; Guo, Z.; Li, M.; Bertling Tjernberg, L. Investigation on Liquid Cold Plate Thermal Management System with Heat Pipes for LiFePO₄ Battery Pack in Electric Vehicles. *Appl. Therm. Eng.* **2021**, *185*, 116382. [[CrossRef](#)]
- Sun, H.; Liu, X.; Liao, H.; Wang, C.; Zhang, J.; Tian, W.; Qiu, S.; Su, G. Experiment Study on Thermal Behavior of a Horizontal High-Temperature Heat Pipe under Motion Conditions. *Ann. Nucl. Energy* **2022**, *165*, 108760. [[CrossRef](#)]
- Mauro, G.M.; Iasiello, M.; Bianco, N.; Chiu, W.K.S.; Naso, V. Mono-and Multi-Objective CFD Optimization of Graded Foam-Filled Channels. *Materials* **2022**, *15*, 968. [[CrossRef](#)] [[PubMed](#)]
- Iasiello, M.; Bianco, N.; Chiu, W.K.S.; Naso, V. The Effects of Variable Porosity and Cell Size on the Thermal Performance of Functionally-Graded Foams. *Int. J. Therm. Sci.* **2021**, *160*, 106696. [[CrossRef](#)]
- Chen, X.; Xia, X.; Sun, C.; Wang, F.; Liu, R. Performance Evaluation of a Double-Pipe Heat Exchanger with Uniform and Graded Metal Foams. *Heat Mass Transf.* **2020**, *56*, 291–302. [[CrossRef](#)]
- Tuckerman, D.B.; Pease, R.F.W. High-Performance Heat Sinking for VLSI. *IEEE Electron Device Lett.* **1981**, *2*, 126–129. [[CrossRef](#)]

9. Saeed, M.; Kim, M.H. Heat Transfer Enhancement Using Nanofluids ($\text{Al}_2\text{O}_3\text{-H}_2\text{O}$) in Mini-Channel Heatsinks. *Int. J. Heat Mass Transf.* **2018**, *120*, 671–682. [[CrossRef](#)]
10. Mohammed Adham, A.; Mohd-Ghazali, N.; Ahmad, R. Thermal and Hydrodynamic Analysis of Microchannel Heat Sinks: A Review. *Renew. Sustain. Energy Rev.* **2013**, *21*, 614–622. [[CrossRef](#)]
11. Khoshvaght-Aliabadi, M.; Nozan, F. Water Cooled Corrugated Minichannel Heat Sink for Electronic Devices: Effect of Corrugation Shape. *Int. Commun. Heat Mass Transf.* **2016**, *76*, 188–196. [[CrossRef](#)]
12. Xu, S.; Li, Y.; Hu, X.; Yang, L. Characteristics of Heat Transfer and Fluid Flow in a Fractal Multilayer Silicon Microchannel. *Int. Commun. Heat Mass Transf.* **2016**, *71*, 86–95. [[CrossRef](#)]
13. Wang, H.; Chen, Z.; Gao, J. Influence of Geometric Parameters on Flow and Heat Transfer Performance of Micro-Channel Heat Sinks. *Appl. Therm. Eng.* **2016**, *107*, 870–879. [[CrossRef](#)]
14. Song, J.; Liu, F.; Sui, Y.; Jing, D. Numerical Studies on the Hydraulic and Thermal Performances of Trapezoidal Microchannel Heat Sink. *Int. J. Therm. Sci.* **2021**, *161*, 106755. [[CrossRef](#)]
15. Kim, B. An Experimental Study on Fully Developed Laminar Flow and Heat Transfer in Rectangular Microchannels. *Int. J. Heat Fluid Flow* **2016**, *62*, 224–232. [[CrossRef](#)]
16. Peng, Y.; Li, Z.; Li, S.; Cao, B.; Wu, X.; Zhao, X. The Experimental Study of the Heat Transfer Performance of a Zigzag-Serpentine Microchannel Heat Sink. *Int. J. Therm. Sci.* **2021**, *163*, 106831. [[CrossRef](#)]
17. Xu, B.; Ooti, K.T.; Wong, N.T.; Choi, W.K. Experimental Investigation of Flow Friction for Liquid Flow in Microchannels. *Int. Commun. Heat Mass Transf.* **2000**, *27*, 1165–1176. [[CrossRef](#)]
18. Ramos-Alvarado, B.; Li, P.; Liu, H.; Hernandez-Guerrero, A. CFD Study of Liquid-Cooled Heat Sinks with Microchannel Flow Field Configurations for Electronics, Fuel Cells, and Concentrated Solar Cells. *Appl. Therm. Eng.* **2011**, *31*, 2494–2507. [[CrossRef](#)]
19. Sohankar, A.; Joulaei, A.; Mahmoodi, M. Fluid Flow and Convective Heat Transfer in a Rotating Rectangular Microchannel with Various Aspect Ratios. *Int. J. Therm. Sci.* **2021**, *172*, 107259. [[CrossRef](#)]
20. Ali, A.M.; Angelino, M.; Rona, A. Numerical Analysis on the Thermal Performance of Microchannel Heat Sinks with Al_2O_3 Nanofluid and Various Fins. *Appl. Therm. Eng.* **2021**, *198*, 117458. [[CrossRef](#)]
21. Farrukh, B.M.; Chen, G.M.; Tso, C.P. Viscous Dissipation Effect on CuO-Water Nanofluid-Cooled Microchannel Heat Sinks. *Case Stud. Therm. Eng.* **2021**, *26*, 101159. [[CrossRef](#)]
22. Tran, N.; Chang, Y.J.; Wang, C.C. Optimization of Thermal Performance of Multi-Nozzle Trapezoidal Microchannel Heat Sinks by Using Nanofluids of Al_2O_3 and TiO_2 . *Int. J. Heat Mass Transf.* **2018**, *117*, 787–798. [[CrossRef](#)]
23. Murali Krishna, V.; Sandeep Kumar, M.; Muthalagu, R.; Senthil Kumar, P.; Mounika, R. Numerical Study of Fluid Flow and Heat Transfer for Flow of Cu- Al_2O_3 -Water Hybrid Nanofluid in a Microchannel Heat Sink. *Mater. Today Proc.* **2022**, *49*, 1298–1302. [[CrossRef](#)]
24. Martínez, V.A.; Lozano-Steinmetz, F.; Vasco, D.A.; Zapata, P.A.; Chi-Durán, I.; Singh, D.P. Thermal Characterization and Stability Analysis of Aqueous ZnO-Based Nanofluids Numerically Implemented in Microchannel Heat Sinks. *Therm. Sci. Eng. Prog.* **2021**, *22*, 100792. [[CrossRef](#)]
25. Chein, R.; Chuang, J. Experimental Microchannel Heat Sink Performance Studies Using Nanofluids. *Int. J. Therm. Sci.* **2007**, *46*, 57–66. [[CrossRef](#)]
26. Jung, S.Y.; Park, H. Experimental Investigation of Heat Transfer of Al_2O_3 Nanofluid in a Microchannel Heat Sink. *Int. J. Heat Mass Transf.* **2021**, *179*, 121729. [[CrossRef](#)]
27. Tu, Y.; Zeng, Y. Flow and Heat Transfer Characteristics Study of Supercritical CO_2 in Horizontal Semicircular Channel for Cooling Process. *Case Stud. Therm. Eng.* **2020**, *21*, 100691. [[CrossRef](#)]
28. Li, W.; Yu, Z. Heat Exchangers for Cooling Supercritical Carbon Dioxide and Heat Transfer Enhancement: A Review and Assessment. *Energy Rep.* **2021**, *7*, 4085–4105. [[CrossRef](#)]
29. Saeed, M.; Berrouk, A.S.; AlShehhi, M.S.; AlWahedi, Y.F. Numerical Investigation of the Thermohydraulic Characteristics of Microchannel Heat Sinks Using Supercritical CO_2 as a Coolant. *J. Supercrit. Fluids* **2021**, *176*, 105306. [[CrossRef](#)]
30. Awais, A.A.; Saeed, M.; Kim, M.H. Performance Enhancement in Minichannel Heat Sinks Using Supercritical Carbon Dioxide (SCO_2) as a Coolant. *Int. J. Heat Mass Transf.* **2021**, *177*, 121539. [[CrossRef](#)]
31. Khalesi, J.; Sarunac, N. Numerical Analysis of Flow and Conjugate Heat Transfer for Supercritical CO_2 and Liquid Sodium in Square Microchannels. *Int. J. Heat Mass Transf.* **2019**, *132*, 1187–1199. [[CrossRef](#)]
32. Saeed, M.; Kim, M.H. Thermal and Hydraulic Performance of SCO_2 PCHE with Different Fin Configurations. *Appl. Therm. Eng.* **2017**, *127*, 975–985. [[CrossRef](#)]
33. Aneesh, A.M.; Sharma, A.; Srivastava, A.; Chaudhury, P. Effects of Wavy Channel Configurations on Thermal-Hydraulic Characteristics of Printed Circuit Heat Exchanger (PCHE). *Int. J. Heat Mass Transf.* **2018**, *118*, 304–315. [[CrossRef](#)]
34. Geyer, P.E.; Fletcher, D.F.; Haynes, B.S. Laminar Flow and Heat Transfer in a Periodic Trapezoidal Channel with Semi-Circular Cross-Section. *Int. J. Heat Mass Transf.* **2007**, *50*, 3471–3480. [[CrossRef](#)]
35. Batchelor, C.K.; Batchelor, G.K. *An Introduction to Fluid Dynamics*; Cambridge University Press: Cambridge, UK, 2000; ISBN 0521663962.
36. Khan, W.A.; Culham, J.R.; Yovanovich, M.M. Optimization of Microchannel Heat Sinks Using Entropy Generation Minimization Method. *IEEE Trans. Compon. Packag. Technol.* **2009**, *32*, 243–251. [[CrossRef](#)]

37. Li, Y.F.; Xia, G.D.; Ma, D.D.; Jia, Y.T.; Wang, J. Characteristics of Laminar Flow and Heat Transfer in Microchannel Heat Sink with Triangular Cavities and Rectangular Ribs. *Int. J. Heat Mass Transf.* **2016**, *98*, 17–28. [[CrossRef](#)]
38. Lee, P.S.; Garimella, S.V.; Liu, D. Investigation of Heat Transfer in Rectangular Microchannels. *Int. J. Heat Mass Transf.* **2005**, *48*, 1688–1704. [[CrossRef](#)]
39. Tu, Y.; Zeng, Y. Heat Transfer and Hydraulic Characteristics of Supercritical CO₂ in Cooled and Heated Horizontal Semicircular Channels. *J. Appl. Fluid Mech.* **2021**, *14*, 1351–1362. [[CrossRef](#)]